

The XMM/2dF survey III: Comparison between optical and X-ray cluster detection methods

S. Basilakos¹, M. Plionis^{1,2}, A. Georgakakis¹, I. Georgantopoulos¹, T. Gaga^{1,3}, V. Kolokotronis¹, G. C. Stewart⁴

¹ *Institute of Astronomy & Astrophysics, National Observatory of Athens, I.Metaxa & B.Pavlou, Palaia Penteli, 152 36, Athens, Greece*

² *Instituto Nacional de Astrofísica, Óptica y Electrónica (INAOE) Apartado Postal 51 y 216, 72000, Puebla, Pue., Mexico*

³ *Physics Department, Univ. of Athens, Panepistimioupolis, Zografou, Athens, Greece*

⁴ *Department of Physics and Astronomy, University of Leicester, UK, LE1 7RH*

22 May 2019

ABSTRACT

We directly compare X-ray and optical techniques of cluster detection by combining SDSS photometric data with a wide-field ($\sim 1.8 \text{ deg}^2$) XMM-Newton survey in the North Galactic Pole region. The optical cluster detection procedure is based on merging two independent selection methods - a smoothing+percolation technique, and a Matched Filter Algorithm. The X-ray cluster detection is based on a wavelet-based algorithm, incorporated in the SAS v.5.2 package. The final optical sample counts 9 candidate clusters with richness of more than 20 galaxies, corresponding roughly to APM richness class. Three, of our optically detected clusters are also detected in our X-ray survey. The most probable cause of the small number of optical cluster candidates detected in our X-ray survey is that they are relatively poor clusters, fainter than the X-ray flux limit (for extended sources) of our survey $f_x(0.3 - 2\text{keV}) \simeq 2 \times 10^{-14} \text{ erg cm}^{-2} \text{ s}^{-1}$.

Keywords: galaxies: clusters: general - cosmology:observations - cosmology: large-scale structure of Universe.

1 INTRODUCTION

Clusters of galaxies occupy an eminent position in the structure hierarchy, being the most massive virialized systems known and therefore they appear to be ideal tools for testing theories of structure formation and extracting invaluable cosmological informations (cf. Bahcall 1988; West Jones & Forman 1995; Böhringer 1995; Carlberg et al. 1996; Borgani & Guzzo 2001; Nichol 2002 and references therein).

The cosmological significance of galaxy clusters has initiated a number of studies aiming to compile unbiased cluster samples to high redshifts, utilizing multi-wavelength data (e.g. optical, X-ray, radio). In order to investigate the global properties of the cosmological background, it is necessary to construct and study large samples of clusters (cf. Borgani & Guzzo 2001). On the other hand, the study of individual clusters, provide complementary information regarding their physical properties and evolutionary processes. Thus, it is very important to fully understand the selection effects that enter in the construction of cluster samples since these could bias the statistical results resulting from the study of these samples (cf. Sutherland 1988).

From the optical point of view there are several

available samples in the literature. For example, the Abell/ACO catalogue (Abell, Corwin & Olowin 1989) was constructed by visual inspection of the Palomar Observatory Sky Survey plates (see also Zwicky, Herzog & Wild 1968 catalogue) and is still playing a key role in astronomical research. Since then, a large number of optically selected samples, constructed with automated methods, have been constructed: EDCC (Lumsden et al. 1992), APM (Dalton et al. 1994), Palomar Distant Cluster Survey (Postman et al. 1996), ESO Imaging Cluster Survey (Olsen et al. 1999), Red-Sequence Cluster Survey (Gladders & Yee 2000) and the SDSS (Sloan Digital Sky Survey) Cluster Survey (Goto et al. 2002; Bahcall et al. 2003). The above cluster samples, based on different selection methods, aim to obtain homogeneously selected optical cluster samples with redshifts that extended beyond the $z \sim 0.2$ limit of the Abell/ACO catalogue. We should mention that the advantage of using optical data is the sheer size of the available cluster catalogues and thus the statistical significance of the emanating results.

A major problem here is that the optical surveys suffer from severe systematic biases which are due to projection effects. Background and foreground galaxies, projected on the cluster could distort the identifications

(e.g. Frenk et al. 1990), which is particularly true for poor systems at high redshifts. X-ray cluster surveys is another possibility, owing to the fact that the diffuse Intra-Cluster Medium (ICM) emits strongly in X-rays. This emission is proportional to the square of the hot gas density, creating a high contrast with respect to the unresolved X-ray background, and thus clusters detected in X-rays are less susceptible to projection effects.

X-ray cluster surveys can be used as an ideal tool for studying the cluster morphology (size, shapes, sub-structures), the Sunyaev Zeldovich effect and finally, evolutionary effects of the X-ray luminosity and temperature functions.

The first such survey, with large impact to the studies of clusters, was based on the Extended Einstein Medium Sensitivity Survey, containing 99 clusters (Stoche et al. 1991). More recently, the *ROSAT* satellite allowed a leap forward in the X-ray cluster astronomy, producing large samples of both nearby and distant clusters (e.g. Castander et al. 1995; Ebeling et al. 1996a, 1996b; Scharf et al. 1997; Ebeling et al. 2000; Böhringer et al. 2001; Gioia et al. 2001; Böhringer et al. 2002; Rosati, Borgani & Norman 2002 and references therein). The most recent *XMM-Newton* observatory with ~ 10 times more effective area and ~ 5 times better spatial resolution than the *ROSAT* provides an ideal platform for the study of galaxy clusters.

However, even with the improved sensitivity of the *XMM-Newton*, optical surveys remain significantly more efficient and less expensive in telescope time for compiling cluster samples, albeit with some incompleteness and spurious detections. The aim of this work is to make a detailed comparison of optical and X-ray cluster identification methods in order to quantify the selection biases introduced by these different techniques and to estimate the possible fraction of spurious optically selected clusters due to projection effects. Throughout this paper we have use $H_0 = 100h^{-1} \text{ km s}^{-1}\text{Mpc}$ and $\Omega_m = 1 - \Omega_\Lambda = 0.3$.

The plan of the paper is as follows. The observed data sets are presented in section 2. In section 3 we discuss the methods employed to identify candidate optical clusters and comment on the systematic effects introduced in our analysis. Also, section 3 describes our projected cluster shape determination method as well as the cluster surface brightness based on a King like profiles. In section 4 we compare the optical and X-ray selected cluster samples. Finally, in section 5, we present our conclusions.

2 OBSERVATIONS

2.1 The SDSS data

In our analysis we use the SDSS Early Data Release (EDR), covering an area of $\sim 400\text{deg}^2$ in the sky (Stoughton et al. 2002). The SDSS is an ongoing imaging and spectroscopic survey and the photometry is obtained in five bands (*ugriz*) to $r \leq 23$ mag. Goto et al. (2002), applied an object cluster finding algorithm to the SDSS EDR and produced a list of galaxy clusters

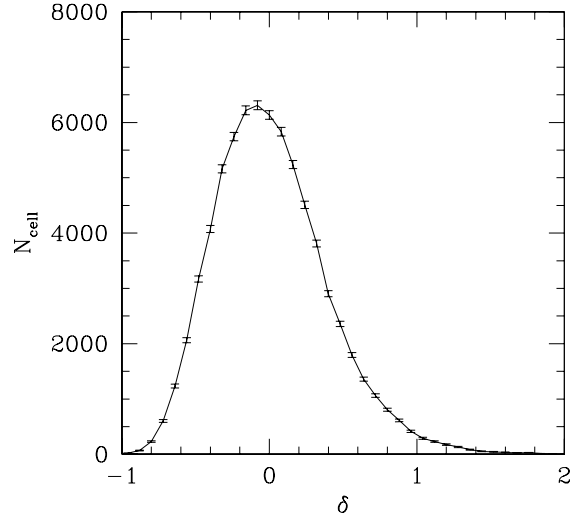


Figure 1. The SDSS probability density function *pdf*.

(hereafter CE catalogue), with estimated photometric redshifts which contains 2770 and 1868 galaxy clusters in the North and South slices, respectively. The cluster redshifts were estimated using color information by identifying the bin in $g - r$ which has the largest number of galaxies around the color prediction of elliptical galaxies (Fukugita, Shimasaku, Ichikawa 1995) at different redshifts (which define the different $g - r$ bins). Note that the true and estimated redshifts are better correlated for $z < 0.3$ (Goto et al. 2002), were the rms scatter is ~ 0.015 , while for $z > 0.3$ it is ~ 0.021 . Note, that the CE method is optimized up to $z \leq 0.4$ and becomes highly insensitive at higher redshifts.

In the present analysis we cross-correlated the Goto et al. (2002) cluster positions with our *XMM* fields (see next section), and found a total of 29 Goto et al. clusters in this area.

2.2 The XMM data

We analyzed 9 *XMM-Newton* fields with nominal exposure time between 2 and 10 ksec. The *XMM-Newton* field-of-view is a circle with a radius of 15 arcmin and thus our survey covers an area of 1.8 deg^2 . However, one of the fields, suffering from significantly elevated and flaring particle background, was excluded from the X-ray analysis. This reduces our effective area to 1.6 deg^2 . The details of the X-ray observations are given in Georgantopoulos et al. (in preparation 2003).

3 CLUSTER DETECTION

Identifying real clusters in two-dimensional data is a difficult problem since projection effects can significantly affect the visual appearance of clusters and distort the true pattern. Many different algorithms have been proposed and applied on different data sets. Here we present

and apply on the subsample of the SDSS data that overlaps with our XMM-*Newton* survey, two methods one of which is new.

3.1 The Smoothing+Percolation Procedure

This cluster detection algorithm is based on smoothing the discrete distribution using a Gaussian smoothing kernel on a $N_{gr} \times N_{gr}$ grid:

$$\mathcal{W}(|\mathbf{x}_i - \mathbf{x}_{gr}|) = \frac{1}{\sqrt{2\pi}R_{sm}^2} \exp\left(-\frac{|\mathbf{x}_i - \mathbf{x}_{gr}|^2}{2R_{sm}^2}\right), \quad (1)$$

with R_{sm} the smoothing radius in grid-cell units and \mathbf{x}_i the Cartesian position of the i^{th} galaxy. The smoothed surface density, of the j th cell at the grid-cell positions \mathbf{x}_{gr} , is then:

$$\rho_j(\mathbf{x}_{gr}) = \frac{\sum_i \rho_j(\mathbf{x}_i) \mathcal{W}(|\mathbf{x}_i - \mathbf{x}_{gr}|)}{\int \mathcal{W}(|\mathbf{x}_i - \mathbf{x}_{gr}|) d^2x}, \quad (2)$$

where the sum is over the distribution of galaxies with positions \mathbf{x}_i . For each cell we define its density fluctuation, δ_j from:

$$\delta_j = \frac{\rho_j(x_{gr}) - \langle \rho \rangle}{\langle \rho \rangle}, \quad (3)$$

where $\langle \rho \rangle$ is the mean projected SDSS galaxy density and the probability density function, $f(\delta)$, which is plotted in Fig. 1. We select all grid-cells with overdensities above a chosen critical threshold ($\delta \geq \delta_{cr}$) and then we use a friends-of-friends algorithm to link all adjacent cells in order to form groups of connected cells, which we consider as our candidate clusters. Note that the grid cell size that we use is such that at $z = 0.4$ it corresponds to $100 h^{-1} \text{kpc}$ ($\sim 19''$).

There are three free parameters in the above procedure; the critical overdensity threshold, δ_{cr} , the smoothing radius, R_{sm} and the number of connected cells (n_c) above which we consider a candidate cluster. Due to the fact that clusters should be identified as high density regions, we choose the critical value of the overdensity to be $\delta_{cr} \simeq 1$ which corresponds to the $\sim 98\%$ -ile value of the probability density function (*pdf*) plotted in Fig.1. Had we used lower values of δ_{cr} we would have percolated overdense regions through large parts of the whole area.

The R_{sm} and n_c parameters were chosen in such a way as to minimize the number of spuriously detected clusters. To this end we perform a series of Monte-Carlo simulations in which we randomize the positions of the SDSS galaxies, destroying its intrinsic clustering, while keeping unchanged the galaxy redshift selection function. On this intrinsically random galaxy distribution we apply the procedure described above, by varying the values of the free parameters (R_{sm} and n_c). We define the probability of detecting real clusters in the SDSS data, as $\mathcal{P}(R_{sm}, n_c) = 1 - N_{rand}/N_{SDSS}$, where N_{rand} is the number of clusters detected in the randomized distribution and N_{SDSS} is the number of clusters detected in the true SDSS data. In Fig. 2 we show as a greyscale these probabilities. Although, increasing R_{sm} and n_c , results in very high probabilities of detecting real high-density

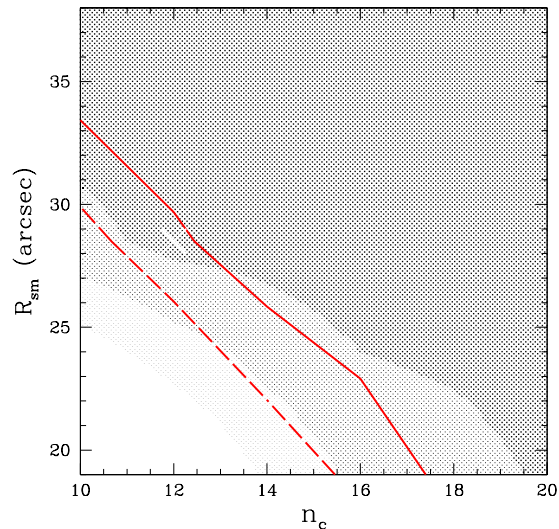


Figure 2. Statistical significance of our cluster detection procedure as a function of the smoothing radius R_{sm} and minimum number of connected cells, n_c . The darkest greyscale corresponds to $\mathcal{P} = 0.96$, while the faintest to $\mathcal{P} < 0.88$. The continuous line corresponds to the expected number of APM clusters, while the broken line to the number Goto et al. (2002) clusters. The cross reflects our best choice of the free parameters (R_{sm} and n_c).

regions, it also results in a very small such number. We therefore attempt to break this degeneracy by using the expected number of clusters from existing surveys. For example, the continuous line in Fig.2 corresponds to the number of expected APM clusters in the area covered by our XMM/2dF survey, while the thick broken line delineates the corresponding number of the Goto et al (2002) clusters. The region of the highest probability, that falls within the above cluster number limits, is that corresponding to:

$$R_{sm} = 28.5'' \quad n_c = 12,$$

which we choose as our optimal parameters for the detection of real clusters.

In Fig. 3 we plot the smoothed SDSS galaxy distribution, using the above value of R_{sm} , on the equatorial plane with a contour step of $\Delta\delta = 0.2$, starting from $\delta_{cr} = 1$. Many overdense regions are apparent. Finally, we note that our cluster finding algorithm (hereafter, SMP method) with $n_c = 12$ produces a list of 25 candidate clusters. Out of these, 11 are common with the Goto et al (2002) sample of 29 clusters in the same region.

3.2 The Matched Filter Algorithm

In addition to the 2D smoothing technique we have also employed the matched filter algorithm (hereafter MFA) described by Postman et al. (1996) to identify optical galaxy overdensities. The advantage of this method is that it exploits both positional and photometric information producing galaxy density maps where spurious galaxy fluctuations are suppressed. Also, an attractive

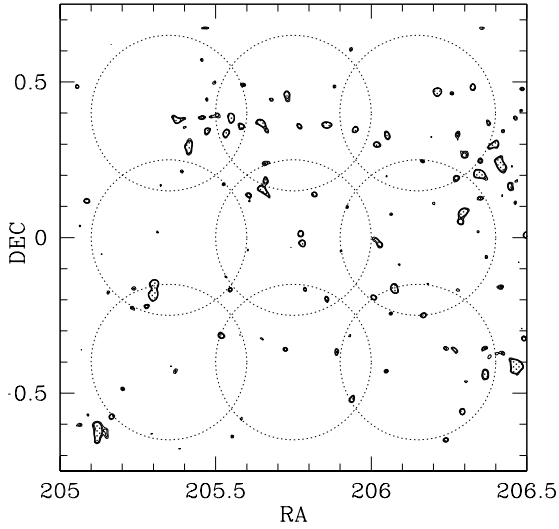


Figure 3. The smooth SDSS density field on equatorial coordinates. The $\delta_{cr} = 1$ level appears as a thick continuous line. The large dotted circles represent the XMM 15 arcmin radius fields of view of our shallow XMM/2dF survey.

feature of this method is that it provides redshift estimates for the detected candidate galaxy clusters. A drawback of the matched filter method is that one must assume a form for the cluster luminosity function and radial profile. Clusters with the same richness but different intrinsic shape, or different luminosity function from the assumed ones do not have the same likelihood of being detected.

A detailed description of the matched filter algorithm can be found in Postman et al. (1996). In brief, the filter used to convolve the galaxy catalogue is derived from an approximate maximum likelihood estimator obtained from a model of the spatial and luminosity distribution of galaxies within a cluster. At any given patch of the sky the number density of galaxies per magnitude bin is

$$D(r, m) = b(m) + \Lambda_{cl} P(r/r_c) \phi(m - m^*) , \quad (4)$$

where $D(r, m)$ is the galaxy surface density (cluster+field galaxies) at a given magnitude m and at a distance r from the galaxy cluster center, $b(m)$ is the field galaxy surface density, $P(r/r_c)$ is the cluster projected radial profile, $\phi(m - m^*)$ is the cluster luminosity function and Λ_{cl} is an estimator of the cluster richness. The parameters r_c and m^* are the characteristic cluster scale length and apparent magnitude corresponding to the characteristic luminosity of the cluster luminosity function. Postman et al. (1996) showed that the filter for cluster detection should maximize the expression

$$\int P(r/r_c) \frac{\phi(m - m^*)}{b(m)} D(m, r) d^2r dm . \quad (5)$$

Assuming that the galaxy distribution $D(m, r)$ can be represented by a series of δ -functions at the observed positions and magnitudes, the integral above is reduced to

$$S(i, j) = \sum_{k=1}^{N_g} P(r_k/r_c) L(m_k) , \quad (6)$$

where $L(m_k)$ is defined as

$$L(m) = \frac{\phi(m - m^*)}{b(m)} . \quad (7)$$

The quantity $S(i, j)$ is the value of the (i, j) pixel of the convolved galaxy density map and N_g is total number of galaxies in the catalogue. $L(m_k)$ is the luminosity weighting function (i.e. flux filter). In practice, the survey area is binned into pixels (i, j) of given size (for the choice of values see below) and the sum in equation 6 is evaluated by iterating through all galaxies in the catalogue. This then is repeated for every pixel of the density map. Both m^* and r_c are a function of redshift and hence $S(i, j)$ also depends on redshift through these parameters. The redshift dependence of m^* also includes a k -correction as discussed in the next section.

The flux filter in equation 7 has a divergent integral at faint magnitudes for Schechter luminosity functions with $\alpha < -1$. To overcome this problem Postman et al. (1996) modified the flux filter by introducing a power-law cutoff of the form $10^{-0.4(m - m^*)}$. Therefore, the flux filter in equation 6 is defined as:

$$L(m) = \frac{\phi(m - m^*) 10^{-0.4(m - m^*)}}{b(m)} . \quad (8)$$

The radial filter in equation 6 is defined:

$$P(r) = \begin{cases} \frac{1}{\sqrt{1+(r/r_c)^2}} - \frac{1}{\sqrt{1+(r_{co}/r_c)^2}}, & \text{if } r < r_{co} \\ 0 & \text{otherwise,} \end{cases} \quad (9)$$

where r_c is the cluster core radius and r_{co} is an arbitrary cutoff radius. Here, we assume $r_c = 100 h^{-1}$ kpc and $r_{co} = 1 h^{-1}$ Mpc. The characteristic absolute magnitude of the luminosity function, in r -band is taken to be $M^* = -20.83 + 5 \log h$ (Blanton et al. 2003). Both the radial and the flux filter are normalized as described in Postman et al. (1996).

3.2.1 The MFA Cluster detection

The matched filter algorithm is applied to a 1.8 deg^2 subregion of the SDSS centered on our XMM/2dF survey. We consider galaxies with magnitudes brighter than $r = 23.0$ mag. At fainter magnitudes the SDSS is affected by incompleteness. The galaxy density map $S(i, j)$ representing the galaxy density map is independently estimated for redshifts between $z_{min} = 0.1$ to $z_{max} = 0.6$, incremented in steps of 0.1. The z_{max} corresponds to the redshift where m^* becomes comparable to the limiting magnitude of the survey. The characteristic luminosity, L^* , the faint end slope of the luminosity function, α , and the cluster core radius, r_c , are assumed to remain constant with redshift.

The conversion from luminosity to apparent magnitude requires an assumption to be made on the k -correction of the galaxies. Here we assume a non-evolving elliptical galaxy model obtained from the Bruzual & Charlot (1993) stellar population synthesis

code (Pozzetti, Bruzual, Zamorani 1996). It is important to emphasize that the choice of k -correction does not significantly affect the cluster detections, but has an impact on the redshift determination.

The pixel size of the galaxy density maps at any redshift is taken to be $\approx 19''$ corresponding to a projected cluster core radius of $r_c = 100 h^{-1}$ kpc at the redshift $z = 0.4$ (see section 3.1). Galaxy density maps are created for redshifts 0.1–0.6 and stored in FITS images. The peaks of the galaxy distribution are detected using SExtractor (Bertin & Arnouts 1996). The mean and the variance of the background are determined using a global value in each likelihood map. The main input parameters are the detection threshold, σ_{det} , given as a multiple of background variance, and the minimum number of pixels, N_{min} for a peak to be extracted as candidate cluster. Simulations have been carried out (see next section) to optimize these parameters and to minimize the number of spurious cluster detections ($\approx 5\%$). We adopt $\sigma_{\text{det}} = 4.0$ while N_{min} is set to the area of a circle with radius $r_c = 100 h^{-1}$ kpc at any given redshift.

The significance of a detection, σ , is defined as the maximum value of all the pixels associated with that detection (i.e. pixels with values above the SExtractor detection threshold), expressed in multiples of the rms noise above the background. The peaks (i.e. candidate clusters) extracted on density maps of different redshifts are matched by positional coincidence using a radius of ≈ 1 arcmin. The approximate redshift of the candidate cluster is taken to be the redshift where the detection significance is maximum.

Within the area of our XMM/2dF survey the MFA method identifies 12 cluster candidates out of which 6 are found also by Goto et al (2002) and 9 are found by our SMP method.

3.2.2 The MFA simulations

Monte Carlo simulations similar to those described in section 3.2 were employed to test the performance of the matched filter algorithm and to establish the best choice of extraction parameters. A total of 100 random galaxy catalogues over an area of 1.8 deg^2 (i.e. similar to that covered by the real catalogue) were produced with the same magnitude distribution as the real dataset. The matched filter algorithm was then applied to these mock catalogues and the SExtractor was used to identify peaks in the derived density maps.

Following Olsen et al. (1999) we minimize the number of spurious detections using the SExtractor parameters N_{min} and σ_{det} as well as other properties of the noise peaks such as the number of redshifts where a peak is detected, n_z . We adopt $\sigma_{\text{det}} = 4$, $N_{\text{min}} = \pi r_c^2$ at any given redshift and we only consider peaks that appear in at least two consecutive redshifts (i.e. $n_z \geq 2$). For this choice of parameters we estimate the spurious cluster contamination to be $\approx 5\%$.

3.3 Our final optically selected cluster sample

We construct our final cluster catalogue by adopting the conservative approach of considering as cluster candi-

dates those identified by the two independent selection methods - the SMP technique, and the Matched Filter Algorithm (MFA) respectively. This sample, which we call SMPMFA, consists of 9 clusters with SDSS richness of more than 20 galaxies, corresponding roughly to APM type clusters. Comparing our final list of 9 clusters with the 29 Goto et al. (2002) clusters, we find 5 in common.

3.3.1 Cluster Shapes

In order to investigate further the reality of our candidate clusters, we have fitted their projected galaxy distribution to a King's profile, since we expect that a galaxy enhancement due to projection effects should have a rather flat profile. The King's profile is given by:

$$\Sigma(\theta) \propto \left[1 + \left(\frac{\theta}{\theta_c} \right)^2 \right]^{-\alpha}, \quad (10)$$

where θ_c is the angular cluster core radius. The slope α is related to β , the ratio of the specific energy in galaxies to the specific thermal energy in the gas, by $\alpha = (3\beta - 1)/2$ and spans the range $0.6 \lesssim \alpha \lesssim 1$ (cf. Bahcall & Lubin 1993; Girardi et al. 1995; Girardi et al. 1998).

In order to quantify the parameters of the fit we perform a standard χ^2 minimization procedure between the measured surface density of each of our clusters and eq.(10):

$$\chi^2 = \sum_{i=1}^n \left[\frac{\Sigma_{\text{data}}^i(\theta) - \Sigma_{\text{King}}^i(\theta, \theta_c, \alpha)}{\sigma^i} \right]^2. \quad (11)$$

In Table 1 we present our cluster positions and the parameters of the King's profile, as well as the χ^2 probability (P_{χ^2}) of consistency between the King's profile and the cluster density profile. All candidate clusters, but one, are well fitted by a King's profile with $P_{\chi^2} \geq 0.14$, while the slope α of the profile is $\simeq 0.7$, corresponding to a β -parameter of $\simeq 0.8$ (cf. Cavaliere & Fusco-Femiano 1976; Jones & Forman 1999). Furthermore, we present the estimated cluster redshifts (either from Goto et al. 2000 or from the MFA method). In one case (cluster No.6) we have the spectroscopic redshift from Couch et al (1991).

For those clusters which are well fitted by a King-like profile we can give an approximation regarding their spatial core radius (r_c). Different studies (Girardi et al. 1995; Girardi et al. 1998), have shown that the radial core radius of Abell clusters has an average value of $\bar{r}_c \simeq 0.10 - 0.15 h^{-1}$ Mpc. Therefore, having an estimate of the cluster redshift, the corresponding core radius can be easily found from $r_c = d_L \tan(\theta_c)$, where d_L is the luminosity cluster distance.

In order to check for possible evolutionary trends regarding the cluster core, we have plotted the core radius as a function of redshift. As shown in Fig.3 we find a significant correlation; the coefficient is ~ 0.60 with the probability of zero correlation being $\leq 10^{-5}$. In the local universe (see the first redshift interval in Fig.3), $0 \leq z \leq 0.15$, the core radius is approximately equal

Table 1. List of the SDSS clusters in the XMM area. The correspondence of the columns is as follows: index number, right ascension RA and declination DEC of the cluster center, cluster ellipticity ϵ and ϕ is the cluster position angle (in degrees), the cross correlation results - the numbers correspond to: 1 - CE method, Goto et al. (2002); 2 - Matched Filter Algorithm; 3 - X-ray extended sources (Gaga et al. in preparation 2003); 4 - Couch et al. (1991). The next columns are: the corresponding redshift, r_c is the corresponding spatial core radius with a 2σ error, χ^2 probabilities (P_{χ^2}) of consistency between the intrinsic cluster density profile and King model. Finally, \mathcal{N}_g is the number of galaxies. Note that the r_c has units of $h^{-1}\text{Mpc}$ and the King profile slope is $\alpha \simeq 0.7$.

Index	RA	DEC	ϵ	ϕ	C.-Correlation	z	r_c	P_{χ^2}	\mathcal{N}_g
1	205.513	-0.316	0.10	113.7	2	0.10 ²	0.10 ± 0.03	0.14	20
2	205.417	0.287	0.56	6.3	1,2,3	0.39 ¹ – 0.40 ²	0.50 ± 0.17	0.003	37
3	205.307	-0.183	0.61	4.7	1,2	0.40 ¹ – 0.60 ²	0.39 ± 0.13	0.73	72
4	205.550	0.378	0.37	170.4	1,2	0.31 ¹ – 0.50 ²	0.52 ± 0.17	0.95	22
5	205.859	0.354	0.37	90.7	2	0.60 ²	0.56 ± 0.19	0.50	25
6	205.770	-0.022	0.10	158.2	2,3,4	0.60 ² – 0.67 ⁴	0.35 ± 0.11	0.98	21
7	206.296	0.078	0.56	22.0	1,2	0.37 ¹ – 0.30 ²	0.42 ± 0.14	0.59	51
8	206.363	-0.438	0.43	3.3	2	0.3 ²	0.46 ± 0.15	0.63	24
9	206.210	0.468	0.10	48.0	1,2,3	0.36 ¹ – 0.3 ²	0.09 ± 0.03	0.46	28

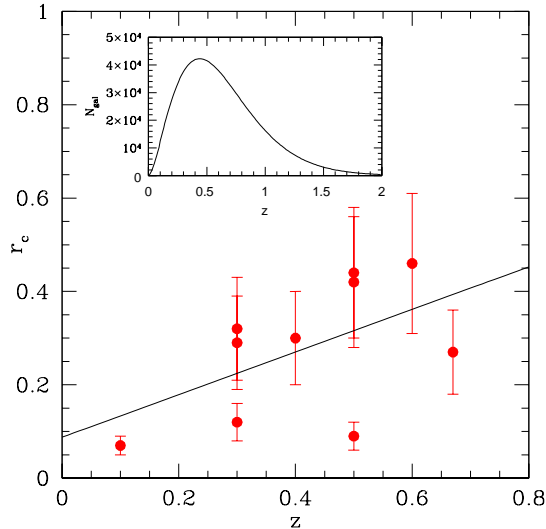


Figure 4. The cluster core radius (r_c) redshift correlation for the analyzed SMPMFA. In the insert we show the SDSS redshift selection function using the Blanton et al (2003) luminosity function.

with $\sim 0.10h^{-1}\text{Mpc}$, which is similar to the value derived by Girardi et al. (1998). The line of the best fit is given by

$$r_c \simeq 0.530(\pm 0.291)z + 0.138(\pm 0.134) . \quad (12)$$

Note that the SDSS redshift selection function increases roughly as $\propto r^3$ up to $z \sim 0.45$ (insert of Fig. 4), which implies that it is roughly volume limited out to this distance and thus the $r_c - z$ trend seen in Fig.4 should not be due to systematic effects related to undersampling of the cluster galaxy population.

We also list in Table 1 the cluster shape parameters determined by using the moments of inertia method (cf. Carter & Metcalfe 1980; Plionis, Barrow & Frenk 1991; Basilakos, Plionis, Maddox, 2001). This method is based in evaluating the moments $I_{11} = \sum \delta_j(r_j^2 - x_j^2)$, $I_{22} = \sum \delta_j(r_j^2 - y_j^2)$, $I_{12} = I_{21} = -\sum \delta_j x_j y_j$, where

δ_j is the galaxy overdensity of each cell and x, y are the Cartesian coordinates of each cell, after transforming the equatorial coordinates into an equal area coordinate system, centered on the cluster center. Then, diagonalizing the inertia tensor

$$\det(I_{ij} - \lambda^2 M_2) = 0 \quad (M_2 \text{ is } 2 \times 2 \text{ unit matrix.}) \quad (13)$$

we obtain the eigenvalues λ_1, λ_2 , from which we define the ellipticity of the configurations under study by: $\epsilon = 1 - \lambda_2/\lambda_1$, with $\lambda_1 > \lambda_2$. The corresponding eigenvectors provide the direction of the principal axis. It is evident that 3 out of 9 clusters have large projected ellipticities ($\epsilon > 0.5$).

3.4 X-ray Cluster Detection

The full details of the cluster detection procedure and the detailed luminosity and temperature results will be described in Gaga et al. (in preparation 2003). Here we only briefly present the main method and results.

In order to detect candidate clusters in our XMM fields we use the soft 0.3-2 keV data since this band maximizes the signal to noise ratio especially in the case of relatively low temperature galaxy clusters. In particular we utilize the *EWAVELET* detection algorithm of the *XMM-Newton SAS v.5.2* analysis software package, which detects sources on the wavelet transformed images.

We searched for sources down to the 5σ detection threshold, separately on the PN and the co-added MOS1 and MOS2 detector images. The output list is fed into the SAS *EMLDETECT* algorithm which performs a maximum likelihood PSF fit on each source yielding a likelihood for the extension. We are using an extension likelihood threshold corresponding to a level of less than 0.5% spurious extended sources. We have detected 7 candidate clusters on the MOS mosaic, while 5 extended sources were detected on the PN images, out of which 3 overlap with the MOS candidates.

We have also eye-balled the candidate clusters and found that in some occasions the detections were due to double or triple nearby point sources. These spu-

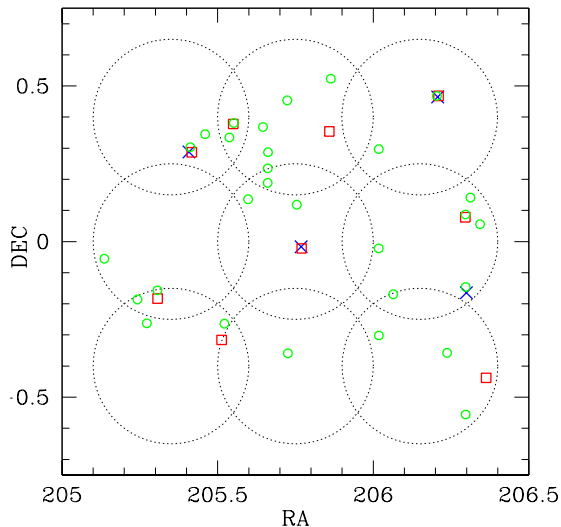


Figure 5. The candidate cluster positions within our shallow XMM-*Newton* survey. Open squares are the optically selected clusters using the SMPMFA technique while open circles are the Goto et al. (2002) clusters. Crosses are X-ray selected clusters of Gaga et al. (in preparation 2003). The large dotted circles represent the 15 arcmin radius XMM fields of view covered by our shallow XMM survey.

rious detections were excluded from our final X-ray based candidate list. This resulted in a final list of 4 X-ray candidates, out of which 2 are detected in both the MOS and PN, one is detected only in the MOS (there was no valid PN image) and one is detected only in the PN. The faintest extended source has a flux of $\sim 2 \times 10^{-14} \text{ erg cm}^{-2} \text{ s}^{-1}$.

In Table 2 we present the properties of the X-ray cluster candidates. Note that the name of the extended source uses the prefix “XMM2DF” followed by the detection (MOS or PN) and the equatorial coordinates.

4 THE OPTICAL VERSUS X-RAY CLUSTER DETECTIONS

We perform a cross-correlation between the different cluster catalogues (optical, X-rays), using a 3 arcmin matching radius to identify common objects. In Fig. 5, we plot the positions of (a) our detected cluster candidates (SMPMFA sample), (b) the Goto et al (2002) clusters and (c) the X-ray detected XMM clusters from Gaga et al. (in preparation 2003). All four X-ray detections coincide with optical cluster candidates from different methods, with the largest coincidence rate (3 out of 9) being with our SMPMFA optical candidates. The most distant cluster in our SMPMFA sample, located at $RA = 13^{\text{h}} 43^{\text{m}} 4.84^{\text{s}}$ $DEC = 00^{\circ} 00' 56.26''$, found also in X-rays, is missed by Goto et al (2002).

The cross-correlation results between the different cluster detection methods are presented in Table 3, which in the first column lists the comparison method pair and in the second column the number of common objects.

It is interesting that our SMPMFA combined method finds 3 out of the 4 X-ray clusters, missing the nearest one, which from its X-ray luminosity appears to be a group of galaxies, rather than a cluster. However, there are still 6 SMPMFA clusters that do not appear to have X-ray counterparts. This could be a hint that these clusters are either the results of projection effects (which however cannot explain the good King profile fits - see Table 1), or that our XMM survey is too shallow to reveal the probably weak X-ray emission from these clusters.

In order to address this issue and to study the relation between the limiting flux of our X-ray survey with respect to exposure time, we have carried out the following experiment. We have analysed observations taken from 15 XMM public fields with mean exposure times ~ 21 ksec in the soft 0.3-2 keV band, after filtering to correct for the high particle background. Using the parameters of the SAS software as described previously, we have detected 31 candidate clusters. The faintest cluster detected, with a flux of $\sim 5 \times 10^{-15} \text{ erg cm}^{-2} \text{ s}^{-1}$, was found in the deepest field with an exposure time of 37 ksec. We then reduce the exposure times to a new mean value of ~ 5 ksec, similar to our shallow survey, and find only 9 out of the 31 previously identified candidate clusters (29%), having a limiting flux of $\sim 2.3 \times 10^{-14} \text{ erg cm}^{-2} \text{ s}^{-1}$ 0.3-2 keV. Therefore, had we had deeper XMM observations (by an average factor of ~ 5 in exposure time) we would have detected ~ 13 X-ray candidate clusters in the region covered by our shallow XMM/2dF survey, which is consistent (within 1σ) with the number of our SMPMFA cluster candidates.

5 CONCLUSIONS

We have made a direct comparison between optical and X-ray based techniques used to identify clusters. We have searched for extended emission in our shallow XMM-*Newton* Survey, which covers a $\sim 1.6 \text{ deg}^2$ area (8 out of 9 original XMM pointings) in the North Galactic Pole region and we have detected 4 candidate X-ray clusters. We have then applied a new cluster finding algorithm on the SDSS galaxy distribution in this region, which is based on merging two independent selection methods - a smoothing-percolation SMP technique, and a Matched Filter Algorithm (MFA). Our final optical cluster catalogue, called the SMPMFA list, counts 9 candidate clusters with richness of more than 20 galaxies, corresponding roughly to APM richness class.

Out of the 4 X-ray candidate clusters 3 are common with our SMPMFA list. This relatively, small number of optical SMPMFA cluster candidates observed in X-rays suggest that some of the optical cluster candidates are either projection effects or poor clusters and hence they are fainter in X-rays than the limit of our shallow survey $f_x(0.3 - 2 \text{ keV}) \simeq 2 \times 10^{-14} \text{ erg cm}^{-2} \text{ s}^{-1}$. This latter explanation seems to be supported from an analysis of public XMM fields with larger exposure times.

Table 2. The X-ray cluster properties: (1) name, (2) X-ray Luminosity (erg s^{-1}) in the 0.3-2 keV band, (3) X-ray flux (0.3-2) keV, in units of $10^{-14} \text{erg cm}^{-2} \text{s}^{-1}$, (4) cluster temperature from Gaga et al. (in preparation 2003), (5) the XMM field, (6) optical follow up and finally, the cluster redshift. Note that the subscripts 1,2 and 4 are the same as in Table 1.

Name	L_x erg s^{-1}	f_x $\times 10^{-14} \text{erg cm}^{-2} \text{s}^{-1}$	$T(\text{keV})$	XMM-Field	Optical	z
XMM2DFPN+MOS J134139.15+001739.33	$10^{42.63}$	1.86	1	F864-1	SMPMFA+CE	0.40 ²
XMM2DFPN+MOS J134304.84-000056.26	$10^{43.60}$	5.55	2	F864-5	SMPMFA	0.67 ⁴
XMM2DFMOS J134511.89-000952.60	$10^{42.00}$	5.05	1	F864-6	CE	0.12 ¹
XMM2DFPN J1344449.68-002753.28	$10^{42.87}$	6.03	1	F864-3	SMPMFA+CE	0.30 ²

Table 3. Cross correlations results. The correspondence of the columns is as follows: comparison pair and the number of common clusters.

Methods compared	Number of common clusters
SMPMFA - CE	5
SMPMFA - X-rays	3
CE - X-rays	3

ACKNOWLEDGMENTS

This work is jointly funded by the European Union and the Greek Government in the framework of the project 'X-ray Astrophysics with ESA's mission XMM'. within the program 'Promotion of Excellence in Technological Development and Research',

REFERENCES

- Abell, G.O., Corwin, H.G., Olowin, R.P., 1989, ApJS, 70, 1
Bahcall, N.A., 1988, ARA&A, 26, 631
Bahcall, N.A., & Lubin, L. M., 1993, ApJ, 415, L17
Bahcall, N.A., et al., 2003, ApJS, in press, astro-ph/0305202
Basilakos S., Plionis M., Maddox S. J., 2001, MNRAS, 316, 779
Bertin, E., & Arnouts, S., 1996, A&AS, 117, 393
Blanton M.R., et al., 2003, ApJ, 592, 819
Böhringer H., 1995, Large Scale Structure in the Universe, Proc. of an International Workshop, Potsdam Germany, 18-24 September 1994. Ed. by Jan P. Mücke, Stefan Gottloeber, and Volker Müller. Singapore: World Scientific, 1995, p.181
Böhringer H., et al. , 2001, A&A, 369, 826
Borgani, S., & Guzzo, L., 2001, Nature, 409, 39
Bruzual A.G., & Charlot, S. 1993, ApJ, 405, 538
Carlberg, R.G., Yee, H.K.C., Ellingson, E., Abraham, R., Gravel, P., Morris, S., Pritchet, C. J., 1996, ApJ, 369, 16
Carter, D. & Metcalfe, J., 1980, MNRAS, 191, 325
Castander, F.J., et al., 1995, Nature, 377, 39
Cavaliere, A., & Fusco-Femiano R., 1976, A&A, 49, 137
Couch, W.J., Ellis, R. S., MacLaren, I., Malin, D. F., 1991, MNRAS, 249, 606
Dalton, G.B., Efstathiou, G., Maddox, S. J., Sutherland, W. J., 1994, MNRAS, 269, 151
Ebeling, H., et al., 1996a, Proc. Roentgenstrahlung from the Universe, MPE, Report 263, ed. H. U. Zimmerman, J. Trümper, H. Yorke (ISSN 0178-1719), 579
Ebeling, H., Voges, W., Böhringer H., Edge, A. C., Huchra, J. P., Briel, U. G., 1996B, MNRAS, 281, 799
Ebeling, H., et al., 2000, ApJ, 534, 133
Frenk, C. S., White, S. D. M., Efstathiou, G., Davis, M., 1990, ApJ, 351, 10
Fukugita, M., Shimasaku, K., Ichikawa, T. 1995, PASP, 107, 945
Gioia, I. M., Henry, J. P., Mullis, C. R., Voges, M., Briel, U. G., Böhringer H., Huchra, J. P., 2001, ApJ, 553, L105
Girardi, M., Biviano A., Giuricin G., Mardirossian F., Mezzetti M., 1995, ApJ, 438, 527
Girardi, M., Giuricin G., Mardirossian, F., Mezzetti M., Boschin W., 1998, ApJ, 505, 74
Gladders, M. D., & Yee, H. K. C., 2000, AJ, 120, 2148
Goto, T., et al., 2002, AJ, 123, 1807
Jones, C., Forman, W., 1999, ApJ, 511, 65
Lidman, C. E., & Peterson, B. A., 1996, AJ, 112, 2454
Lumsden, S. L., Nichol, R.C., Collins, C. A., Guzzo, L., 1992, MNRAS, 258, 1
Nichol, R. C., 2002, in ASP Conf. Ser., Tracing Cosmic Evolution with Galaxy Clusters, ed. S. Borgani, M. Mezzetti, R. Valdarnini, 268, 57
Olsen, L. F., et al., 1999, A&A, 345, 681
Plionis M., Barrow J.D., Frenk, C.S., 1991, MNRAS, 249, 662
Postman, M., Lubin, L. M., Gunn, J. E., Oke, J. B., Hoessel, J. G., Schneider, D. P., Christensen, J. A., 1996, AJ, 111, 615
Pozzetti, L., Bruzual A., G., Zamorani, G., 1996, MNRAS, 281, 953
Rosati, P., Borgani, S., Norman, C., 2002, ARA&A, 40, 539
Scharf, C. A., Jones, L. R., Ebeling, H., Perlman, E., Malkan, M., Wegner, G., 1997, ApJ, 477, 79
Stocke, J. T., Morris, S. L., Gioia, I. M., Maccacaro, T., Schild, R., Wolter, A., Fleming, T. A., Henry, J. P., 1991, ApJS, 76, 813
Stoughton, C., et al., 2002, AJ, 123, 485
Sutherland, W., 1988, MNRAS, 234, 159
West, M. J., Jones, C., Forman, W., 1995, ApJ, 451, L5
York, D. G., et al., 2000, AJ, 120, 1579
Zwicky, F., Herzog, E., Wild, P., 1968, Pasadena: California Institute of Technology (CIT), 1961-1968